THE JOURNAL OF PHYSICAL CHEMISTRY C

Article

pubs.acs.org/JPCC

Effect of Solvent Additive on Generation, Recombination, and Extraction in PTB7:PCBM Solar Cells: A Conclusive Experimental and Numerical Simulation Study

Juliane Kniepert,[†] Ilja Lange,[†] Jan Heidbrink,[†] Jona Kurpiers,[†] Thomas J. K. Brenner,[†] L. Jan Anton Koster,[‡] and Dieter Neher*[,†]

[†]Institute of Physics and Astronomy, University of Potsdam, Karl-Liebknecht-Strasse 24-25, 14476 Potsdam, Germany

[‡]Zernike Institute for Advanced Materials, University of Groningen, Nijenborgh 4, 9747, AG, Groningen, The Netherlands

Supporting Information

ABSTRACT: Time-delayed collection field (TDCF), bias-assisted charge extraction (BACE), and space charge-limited current (SCLC) measurements are combined with complete numerical device simulations to unveil the effect of the solvent additive 1,8-diiodooctane (DIO) on the performance of PTB7:PCBM bulk heterojunction solar cells. DIO is shown to increase the charge generation rate, reduce geminate and bimolecular recombination, and increase the electron mobility. In total, the reduction of loss currents by processing with the additive raises the power conversion efficiency of the PTB7:PCBM blend by a factor of almost three. The lower generation rates and higher geminate recombination losses in devices without DIO are consistent with a blend morphology comprising large fullerene clusters embedded within a PTB7-rich matrix, while the low electron mobility suggests that these fullerene clusters are themselves composed of smaller pure fullerene aggregates separated by disordered areas. Our device simulations show unambiguously that the effect of the additive on the shape of the current−voltage curve (J−V) cannot be ascribed to the variation of only the mobility, the recombination, or the field dependence of generation. It is only when the changes of all three parameters are taken into account that the simulation matches the experimental J−V characteristics under all illumination conditions and for a wide range of voltages.

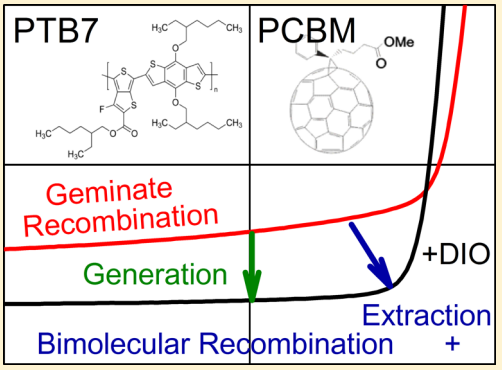

1. INTRODUCTION

Organic solar cells have experienced significant efficiency improvements in recent years, mainly due to the development of new low-band-gap copolymers with optimized absorption spectra. Among these polymers, bulk heterojunction (BHJ) solar cells comprising the donor polymer thieno[3,4-*b*]-thiophene-*alt*-benzodithiophene (PTB7) and the fullerene acceptor [6,6]-phenyl C_{71} butyric acid methyl ester (PCBM) yielded a record power conversion efficiency of 9.2%.[1] It was shown that the device properties depend largely on the processing conditions. In particular, the photovoltaic performance improved dramatically when adding 1,8-diiodooctane (DIO) to the blend solution.[2] Consistently, several publications reported a large increase of the short-circuit current density (J_{SC}) and fill factor (FF) when using the solvent additive DIO in PTB7:PCBM blends. This was attributed to an optimized phase-separated structure. A large effect of the morphology on the charge carrier dynamics and the overall performance of the devices has been shown for various polymer:fullerene blends.[3−8] Surprisingly, although the change in nanomorphology of the PTB7:PCBM blend upon addition of DIO has been extensively discussed in the literature,[9−13] comparatively few publications deal with the impact on the charge carrier dynamics. Transient photocurrent measurements in conjunction with numerical simulations by McNeill and co-workers revealed severe charge trapping with increased trap-assisted recombination closer to open circuit in blends of PTB7 with $PC_{71}BM$ processed without additives, which was reduced by the use of DIO.[14] Foertig et al. used transient photovoltage (TPV), charge extraction (CE), and time-delayed collection field (TDCF) measurements to analyze geminate and nongeminate recombination losses in PTB7:$PC_{71}BM$ (1:1.5) blends.[15] This study revealed a more pronounced field dependence of generation without DIO. Interestingly, the combination of TPV and CE data showed similar carrier lifetimes of ca. 4 μs for both blends at V_{oc} and 1 sun illumination but a 2-fold larger steady state charge carrier concentration for the device with DIO, from which a smaller nongeminate recombination rate coefficient would be concluded. However, these data failed to explain the J−V characteristics of the devices without additive and led to a strong overestimation of the performance. To explain this phenomenon, Foertig et al. proposed that a certain

Received: December 20, 2014
Revised: March 16, 2015
Published: March 18, 2015

DOI: 10.1021/jp512721e
J. Phys. Chem. C 2015, 119, 8310−8320

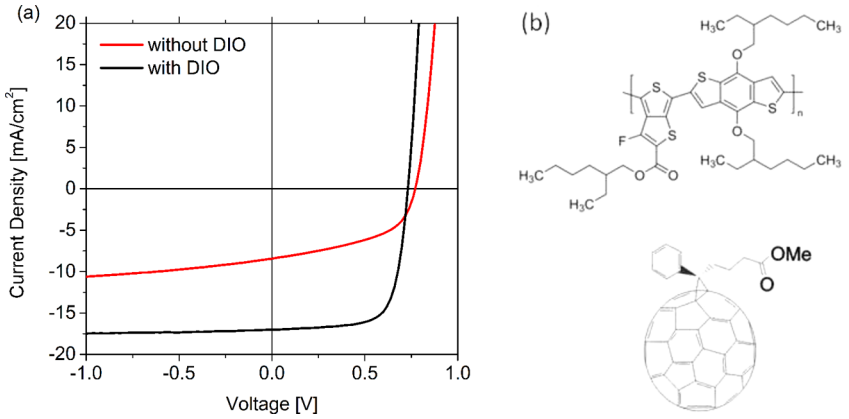

Figure 1. (a) Current–voltage characteristics of PTB7:$PC_{71}BM$ solar cells processed with and without the additive 1,8-diiodooctane (DIO). (b) Chemical structures of PTB7 (top) and $PC_{71}BM$ (bottom).

fraction of photogenerated charge becomes trapped on isolated domains in the blends processed without DIO. These trapped charges could recombine with mobile charge, thus increasing the nongeminate recombination rate, but they would not be observed in CE experiments at short-circuit conditions. In fact, the $J-V$ curve of the device without additive could be reconstructed by assuming a higher total charge density. However, due to possibly incomplete extraction of all charges in these experiments, no information on the nongeminate recombination (NGR) coefficient was supplied in this study. A recent publication by Foster et al. reported a very detailed study on the charge carrier mobility of PTB7:$PC_{61}BM$ prepared with and without DIO.[16] For typical fullerene concentrations used in high-performance devices, the addition of DIO reduced the electron mobility by a factor of 3–4, while the hole mobility was unaffected. This study also stated similar carrier lifetimes and carrier densities for both blends at V_{oc} and 1 sun illumination, indicating very similar rates for nongeminate recombination. The authors concluded that charge collection is not improved with DIO and that the improved performance of the blend processed with DIO is entirely due to suppressed geminate recombination. Unfortunately, device simulations supporting the proposed mechanisms were not supplied in this paper. Notably, Foster et al. studied blends of PTB7 with $PC_{61}BM$, in contrast to most publications dealing with PTB7:$PC_{71}BM$ mixtures. Compared to blends with $PC_{71}BM$, these devices yield a smaller FF, indicating that differences in the charge carrier dynamics cannot be ruled out. Indeed, the steady state carrier density at V_{oc} and 1 sun illumination intensity measured by Foster et al. without the additive is ca. 3 times higher than the value reported by Foertig et al., indicative of different extraction and/or recombination dynamics.

The $J-V$ characteristics of solar cells are determined by free charge carrier generation via dissociation of charge transfer states in competition with geminate recombination and by the efficiency of carrier extraction in competition with nongeminate recombination. Therefore, the characterization of only generation and recombination or the study of only charge carrier mobilities, as was done in most previous studies, leads to an incomplete picture. Rather, a thorough analysis of all dynamic processes in the device is needed. In a recent study on the benchmark system P3HT:PCBM (poly(3-hexylthiophene): [6,6]-phenyl C_{71} butyric acid methyl ester) we were able to show that a careful and comprehensive experimental analysis of charge generation and recombination as a function of bias and intensity combined with drift diffusion simulations provides a deep understanding of the charge carrier dynamics and allowed us to identify the most relevant loss channels.[17]

In this paper we combine TDCF, bias-assisted charge extraction (BACE), and space charge-limited current (SCLC) measurements together with complete numerical device simulations to investigate charge carrier generation, recombination, and extraction. From this we gain an unprecedented deep understanding of the dynamic quantities determining the steady state $J-V$ characteristics of PTB7:PCBM solar cells prepared with and without the solvent additive DIO. We find that DIO increases the overall generation rate, reduces geminate and bimolecular recombination, and increases the electron mobility. In contrast to previous studies it is shown that each of those changes is rather moderate and cannot for itself explain the huge improvement of the power conversion efficiency (PCE) by a factor of almost 3. For the first time, a unified study is presented that separately measures charge carrier generation, recombination, and transport in real operating PTB7:PCBM devices to obtain a complete and conclusive picture about the charge carrier dynamics. The device simulations support our measurements by using the experimental device parameters to exactly reproduce the measured $J-V$ characteristics. The results of experiments and simulations are also discussed in terms of the blend morphology based on extensive studies present in the literature.

2. RESULTS AND DISCUSSION

2.1. Photovoltaic Response and Charge Carrier Generation. Figure 1a shows the $J-V$ characteristics of 1:1.5 by weight PTB7:PCBM devices (chemical structures in Figure 1b) prepared with and without the solvent additive DIO under solar illumination (Oriel Sol 2A solar simulator, AM 1.5 G at 100 mW cm^{-2}). The addition of DIO significantly improves device performance as previously reported.[2,5,15] The power conversion efficiency (PCE) is raised by almost a factor of 3 from 3.3% to 9.1%, which is mainly caused by an increase in FF from 49.7% to 71.5% and J_{SC} from 8.5 to 17.1 mA cm^{-2}. Note that the pixel size of the active area of these devices was 1 mm^2 as a small sample capacity was required to obtain a high temporal resolution of the transient experiments. Devices with larger pixel sizes usually showed a slightly reduced FF and PCE.

In case of a weak voltage dependence of the photocurrent density and negligible nongeminate recombination at high reverse bias, information about charge generation at reverse

DOI: 10.1021/jp512721e
J. Phys. Chem. C 2015, 119, 8310–8320

bias can be obtained directly from the $J-V$ curve. As can be seen from the graph in Figure 1 the photocurrent at high reverse voltages saturates at different values for the devices with or without DIO (see Supporting Information for $J-V$ curves with larger voltage range). This effect denotes a difference in the generation rates for the two devices. With the help of the continuity equation, eq 1, under neglect of nongeminate recombination

$$G = \frac{J_{sat}}{ed} \tag{1}$$

and the measured saturated current density at −3 V (J_{sat}) the generation rates are calculated as 1.1×10^{28} m^{-3} s^{-1} for the device with DIO and 7.3×10^{27} m^{-3} s^{-1} for the device without DIO. A lower generation rate for devices without DIO is in accordance with a larger phase separation in those blends implying a smaller donor−acceptor (DA) interface for exciton splitting. Several groups reported a large phase separation in pristine blends with domains in the order of >100 nm and showed that the main effect of DIO is to suppress the formation of the large fullerene clusters, leading to a smaller length scale of the polymer and fullerene phases and an increase of the effective interfacial area.[2,9−13] Our measurements are in agreement with these reports. A difference in the generation rates was also observed by Chen et al.;[9] however, the absolute values determined in this reference are lower in accordance with a lower short-circuit current density and overall efficiency of their devices. Notably, though the generation rate without DIO is considerably smaller than that with DIO, the photon absorption efficiency is equal in both blends (see Supporting Information for the absorption spectra), meaning that the internal quantum efficiency is reduced in blends without DIO.

It has been shown for several high-performance materials that the generation rate can be dependent on the applied voltage.[8,18] To address a possible field dependence of the free carrier generation, TDCF experiments were performed on the same devices. TDCF is a well-established method to study charge generation in BHJ solar cells.[8,17,19−21] Here, charge carriers are photogenerated with a nanosecond laser pulse and subsequently extracted with a constant high reverse voltage V_{coll}, which is applied after a short delay time. V_{coll} is chosen to be high enough to collect all free charge carriers. By applying different voltages, V_{pre}, relevant for solar cell operation during the laser pulse, the bias-dependent efficiency of free carrier formation in competition to geminate recombination can be probed. Figure 2a shows the total extracted charge Q_{tot} calculated by integrating the photocurrent transients, normalized to the respective value at −2 V. Data from experiments, performed at an excitation density of 0.05 μJ cm^{-2} at 500 nm, were recently published in ref 15. Here, we reuse the results for the following analysis and discussion. The measurements reveal a field-independent generation rate for the devices prepared with DIO in accordance with the very high fill factors in those devices. In contrast, the devices prepared without DIO show a significant field dependence of the free charge generation efficiency. Here about 20% less charge is generated at open-circuit voltage (V_{OC}) compared to −2 V. A linear dependence of Q_{tot} on pulse fluence (see Supporting Information) proves that nongeminate recombination is absent during the delay and extraction and the field dependence can be attributed to geminate recombination only. The inset of Figure 2a displays the original data. It is obvious that more charge is extracted from the devices with additive. This is in agreement with the higher generation rate determined from the $J-V$ curves. The generation rates determined with eq 1 and the field dependence of generation from Figure 2a are later combined to serve as input parameters for the numerical device simulation.

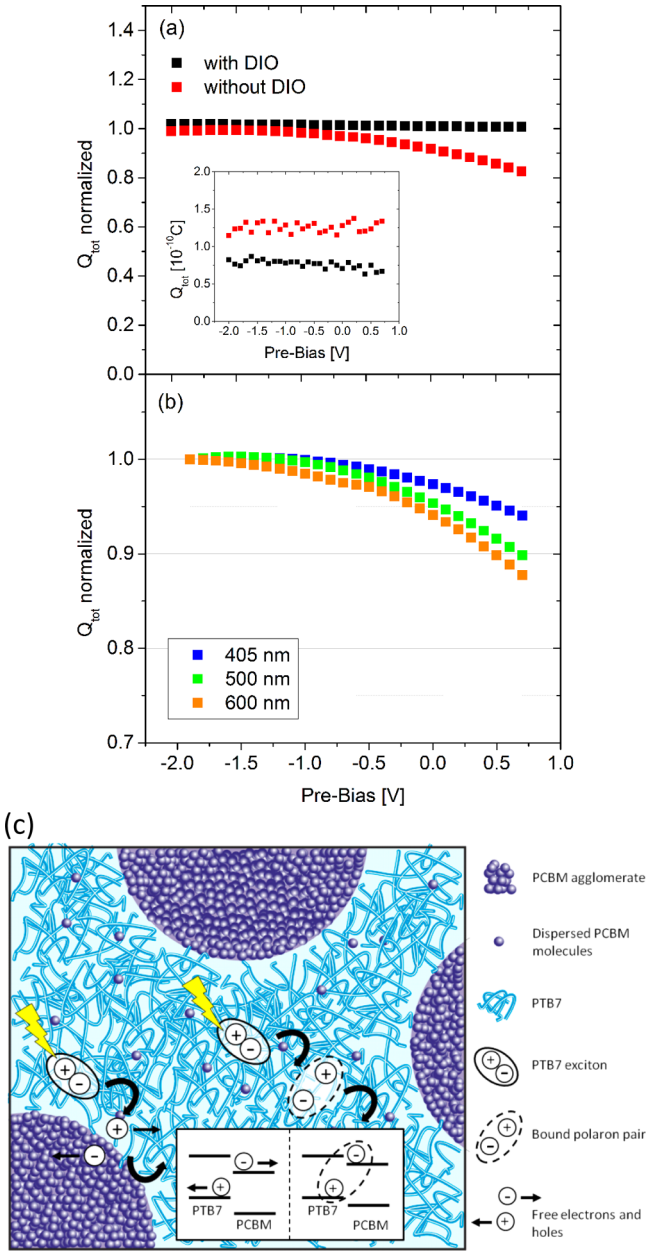

Figure 2. (a) Total extracted charge (Q_{tot}) measured by TDCF as a function of the applied prebias during laser excitation, smoothed, and normalized to Q_{tot} at −2 V. The excitation density was 0.05 μJ cm^{-2} at 500 nm, and the time delay between laser and extraction pulse was 10 ns. (Inset) Raw data. Data is replotted from ref 15. (b) Charge carrier generation of a device without DIO at 3 different wavelengths. The field dependence is stronger if PTB7 is predominantly excited (600 nm, orange) as compared to PCBM excitation (400 nm, blue). (c) Schematic image of the morphology in devices without DIO according to structural studies by Collins et al.[11] Charge generation is field independent close to the agglomerate interfaces and field assisted in the matrix where only dispersed PCBM molecules are available for charge transfer.

In addition, the field dependence of the generation in pristine devices was investigated for different excitation wavelengths (Figure 2b). Note that the overall field dependence in Figure

DOI: 10.1021/jp512721e
J. Phys. Chem. C 2015, 119, 8310−8320

2b is slightly smaller than that in Figure 2a, as these experiments were performed later on a blend with a different batch of PTB7. This batch was purchased from the same supplier (with nominally the same molecular weight). The $J-V$ curves of devices made from this second batch are shown in the Supporting Information. They display slightly better performances but with a very similar effect of the additive on the photovoltaic properties. We observe a smaller field dependence of generation at 405 nm, where PCBM is predominantly excited (see Supporting Information for absorption spectra of PCBM and PTB7). Here, about 5% less charges are generated at V_{OC} compared to −2 V. In contrast, if PTB7 excitation dominates (600 nm) the generation rate drops approximately by 12% when going from reverse bias to open-circuit conditions. This observation is consistent with a recent study by Brenner et al.[22] reporting a stronger voltage dependence of the polymer photocurrent generation in the devices without additive by means of voltage-dependent EQE measurements. Brenner et al. attributed this effect to differences in the nature of the interfacial electron−hole pair, formed at the same DA interface upon excitation of either the polymer or the fullerene. In fact, a larger field dependence of generation upon polymer excitation might indicate that a significant fraction of initially excited polymer excitons form bound charge transfer (CT) states across the interface, which need the aid of an electric field to be fully separated. We propose an alternative explanation, motivated by the large inhomogeneity of the blend morphology without the additive. As pointed out above, work by Collins et al. suggested that blends without DIO consist of pure, agglomerated fullerene domains in the order of 100−200 nm in size, which are embedded in a polymer-rich matrix containing 30% dispersed PCBM. Because of this intermixing and the large dimension of phase separation, well exceeding the exciton diffusion length, a significant fraction of excitons generated on PTB7 chains are not able to reach the heterojunction to the pure fullerene interface but are rather quenched at dispersed PCBM molecules within the matrix. It was shown recently that fullerene agglomerates have a deeper lying LUMO than individual molecules dispersed in a matrix, leading to a higher LUMO offset between donor and acceptor, thereby reducing the probability of geminate or nongeminate recombination.[23] Other studies suggested that the presence of fullerene aggregates leads to strong electron delocalization and ultrafast long-range charge separation.[24−26] In either case, charge transfer states between polymer chains and dispersed fullerenes in large and highly intermixed domains, with no fullerene agglomerates in close vicinity, are expected to suffer from geminate recombination and a higher field dependence of charge separation (Figure 2c schematically illustrates this situation). On the other hand, when excitons are generated on the PCBM clusters, CT generation and split up will occur predominately at the heterojunction between a pure fullerene aggregate and a polymer-rich domain, where free charge formation is expected to be more efficient and less bias dependent.

In blends with DIO the fullerene and polymer domains are in the order of 30 nm in size.[11] Therefore, an agglomerate interface is always within the reach of the exciton diffusion length, and all quenched excitons are efficiently separated into free charge carriers. Consequently, the generation rate is not expected to depend on the electric field in those devices. The results of our TDCF measurements are consistent with these morphology models.

2.2. Bimolecular Recombination versus Charge Extraction. Having thoroughly discussed the carrier generation in the devices, we now turn to the competition of nongeminate recombination and charge extraction which mainly determines the specific shape of the $J-V$ characteristics. At open-circuit conditions, by definition, the net current density is zero, and in the case of bimolecular recombination, a steady state recombination constant can be determined using

$$G = R = k(n)n^2 \tag{2}$$

where G is the generation rate, R is the recombination rate, n is the charge carrier density, and k the bimolecular recombination (BMR) coefficient. Note that this coefficient itself might depend on carrier density and electric field. Using eq 2 is an elegant way to determine $k(n)$, provided that information about the charge carrier density at V_{OC} and the generation rate can be deduced from independent experiments.[27,28]

Following our earlier work,[17,29] BACE was used to determine the carrier density at open-circuit voltage with high accuracy. In a BACE experiment, the device is held at a fixed bias that corresponds exactly to the open-circuit voltage while being illuminated with a certain steady state illumination intensity. When switching off the LEDs, the external bias is rapidly changed to reverse direction. Integration of the photocurrent transient then yields the total mobile charge present in the device. We have previously shown[17] that the application of a reverse extraction bias is crucial for correct determination of the carrier density in a charge extraction (CE) experiment. Especially in devices with high recombination or slow extraction, conventional CE, where the only driving force at short circuit is the built-in field, can easily underestimate the true carrier density. The necessary reverse extraction bias needs to be determined for each individual device (see Figure S5, Supporting Information) and amounted to −2.5 V in the current studies.

With the generation rate being known, the charge carrier density at V_{oc} measured for different illumination intensities then yields information about the apparent recombination order in the device (inset Figure 3a). The slope of the log−log plot equals to 0.45 for the device with DIO, indicating that nongeminate recombination dynamics is a second-order process. Consequently, the recombination coefficient shows only a very weak dependence on the charge carrier density. In contrast, for the device without DIO, the charge carrier density increases with illumination intensity with a slope of 0.31. This points to an apparent third-order recombination process which was often attributed to bimolecular recombination with a carrier density-dependent recombination coefficient.[30]

Figure 3a plots the mean bimolecular recombination coefficient, which assumes that the extracted charge is homogeneously distributed across the entire layer thickness. While in devices with DIO k changes very little with carrier density in the investigated range, it increases almost linearly with n for the sample prepared without the additive. Overall, recombination without DIO is faster than with DIO, except for very small carrier densities. For 1 sun illumination intensity (corresponding to 100 mW/cm^2) the BMR coefficient is $k = 3 \times 10^{-17}$ m^3 s^{-1} (without DIO) and $k = 1.2 \times 10^{-17}$ m^3 s^{-1} (with DIO). Our values for k with DIO are in good agreement to recombination coefficients reported recently by Deledalle et al. for ca. 90 nm thick DIO-processed PTB7:PC$_{71}$BM blends for carrier concentrations above 10^{22} m^{-3}.[31] In contrast, Rauh et al. reported a relatively pronounced increase of k with carrier

DOI: 10.1021/jp512721e
J. Phys. Chem. C 2015, 119, 8310−8320

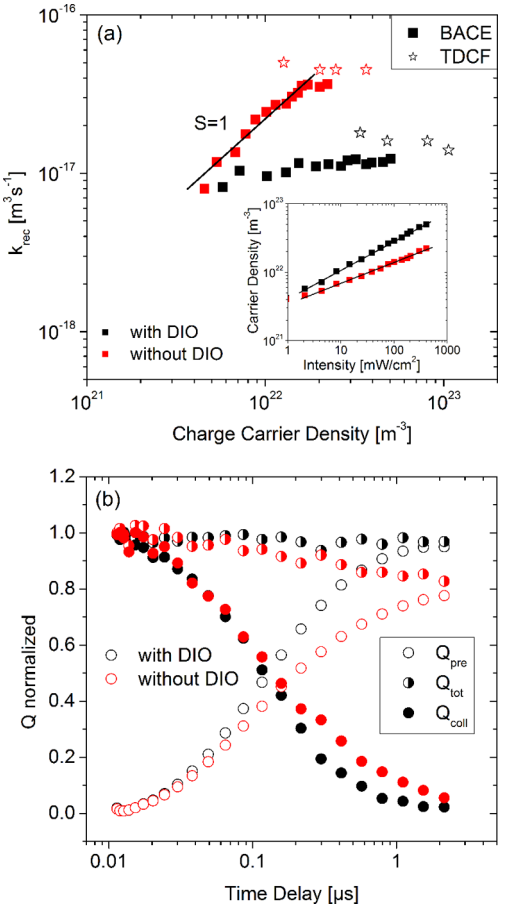

Figure 3. (a) Squares: Steady state BMR coefficients as a function of charge carrier density measured with BACE. The straight line indicates a slope of 1. Stars: Transient BMR coefficients determined with TDCF as a function of the initial generated carrier density. (Inset) Steady state charge carrier densities at open-circuit conditions for different illumination intensities determined by BACE. The straight lines indicate a slope of 0.45 for the device prepared with DIO and a slope of 0.31 for the device without DIO. (b) Normalized Q_{coll}, Q_{pre}, and Q_{tot} measured with TDCF as a function of time delay between laser pulse and extraction pulse. The pulse fluence was 0.2 μJ/cm^2, and the prebias was 0 V. Data show less efficient extraction at short circuit for the device without DIO.

density also for DIO-processed devices, with k ranging between 2×10^{-18} and 8×10^{-18} m^3 s^{-1} for n increasing from 1.5×10^{22} to 4×10^{22} m^{-3} at 300 K.[28] The reasons for the different carrier density dependencies and lower absolute values of k seen by Rauh et al. are yet not understood, but they might (in part) be due to the different techniques used to determine the steady state carrier density, which was CE in ref 28 and is BACE in this work.

A dependence of k on carrier density was initially attributed to a density-dependent mobility in the presence of a broadened DOS due to increased energetic disorder or traps.[27,32] However, work by Deledalle et al. showed that an inhomogeneous spatial distribution of charge carriers in the device results in an apparent density dependence of the mean recombination coefficient.[31] In steady state conditions, an inhomogeneous charge distribution becomes especially critical at thin layer thicknesses and for unbalanced charge carrier mobilities. As a consequence, when the mean carrier density is determined on the basis of CE experiments, the apparent recombination orders can deviate significantly from the order of the local recombination process.[33] In fact, Deledalle et al. showed that for low carrier densities and thin devices a steep increase of $k(n)$ becomes visible, similar to what we observe for the device without DIO, which is most probably caused by the inhomogeneous carrier distribution at low illumination intensities. Also, Deibel and co-workers pointed out that a weak overlap of the photogenerated electron and hole profiles in a device under steady state illumination leads to an underestimation of k, meaning that the value of the mean recombination coefficient is smaller than the true (local) coefficient.[34] Therefore, the dependence of k on carrier density n as deduced from CE experiments needs to be considered with great care.

To address this point further, TDCF measurements were performed with different time delays between the laser pulse and the extraction pulse. Compared to the determination of k from steady state measurements, TDCF has the advantage that a relatively homogeneous charge carrier profile is generated in the device, with perfect overlap between the photogenerated electron and the hole density profiles. This circumvents the problems discussed above. We find that the recombination coefficients extracted from TDCF experiments vary only weakly with carrier density for the two types of blends. Also, for both devices, values for k determined by TDCF agree quite well with recombination coefficients from steady state measurements at high carrier densities. This suggests that the apparent higher recombination order for the device without DIO must, indeed, be related to the particular morphology or an inhomogeneous carrier distribution. Therefore, in the following analysis k was assumed to be independent of carrier density. In fact, as shown below, good fits to the $J-V$ characteristics for all light intensities were possible without the explicit consideration of energetic disorder and for a constant recombination coefficient, implying that the apparent dependence of the mean k on carrier density, as suggested by CE experiments, does not reflect the actual microdynamics in the device.

A second advantage of TDCF is that recombination can also be investigated under different prebias conditions. Even though in the case of PTB7:PCBM no significant dependence of k on prebias was measured (data not shown), an important observation was made from the dynamics at 0 V (short circuit). Figure 3b displays the collected charge, Q_{coll}, the total charge, Q_{tot}, and the precharge, Q_{pre}, as measured with TDCF for increasing time delay. Despite a very similar decay of the collected charge over time, the development of Q_{tot} and Q_{pre} differs for the devices with and without DIO. In the pristine blends less precharge is extracted in the same time span, and therefore, Q_{tot} shows a significant decay, whereas in blends with DIO Q_{tot} stays constant over the whole period. This indicates slower and less efficient charge extraction in the devices without DIO.

The direct measurement of charge carrier mobilities in a working device is quite challenging, and the results might depend strongly on the measurement conditions.[35] One possibility is to determine mobilities from TDCF transients by extrapolating the initial photocurrent slope to zero.[8,36] This method is straightforward and has the advantage that the laser intensity can be chosen such that the resulting carrier density is close to the carrier density of a working solar cell. The drawback of this method is that it does not allow one to differentiate between electron and hole mobility. However, the initial slope of the transient can be used to determine the

DOI: 10.1021/jp512721e
J. Phys. Chem. C 2015, 119, 8310−8320

mobility of the faster carrier type. Figure 4 (inset) shows the mobilities as a function of electric field for devices prepared with and without DIO. The absolute value of the mobility of the faster carrier type (holes) does not change significantly upon addition of DIO in the displayed field range. From this plot a constant mobility of 4.5×10^{-4} $cm^2/(V\ s)$ was determined for the device with DIO and a field-dependent mobility with a zero-field mobility of $\mu_{h0} = 1.2 \times 10^{-3}$ $cm^2/(V\ s)$ and a Poole–Frenkel factor of -0.002 $(cm/V)^{1/2}$ was determined. These numbers were adopted as they stand in the numerical simulation described below.

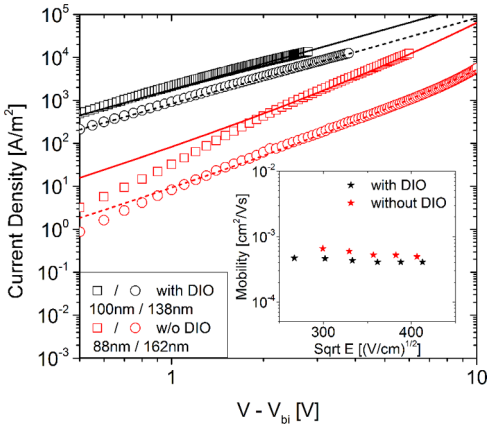

Figure 4. Dark current density–voltage data of electron-only devices prepared with (black) and without (red) DIO for 2 different thicknesses each. Solid and dashed lines are best fits according to eq 6, yielding the following electron mobilities and Poole–Frenkel factors: with DIO $\mu = 4.5 \times 10^{-4}$ $cm^2/(V\ s)$, $\beta = 0$ (100 nm), $\mu = 5.5 \times 10^{-4}$ $cm^2/(V\ s)$, $\beta = 0$ (138 nm); without DIO $\mu = 5.5 \times 10^{-6}$ $cm^2/(V\ s)$, $\beta = 0.003$ $(cm/V)^{1/2}$ (88 nm), $\mu = 4.5 \times 10^{-6}$ $cm^2/(V\ s)$, $\beta = 0.0025$ $(cm/V)^{1/2}$ (162 nm). (Inset) Charge carrier mobilities determined from extrapolating TDCF transients. For the device with DIO (black) a field-independent (hole) mobility of 4.5×10^{-4} $cm^2/(V\ s)$ was determined, while the device without DIO (red) was fitted with a field-dependent mobility, yielding a Poole–Frenkel prefactor of -0.002 $(cm/V)^{1/2}$ and a zero-field mobility of 1.2×10^{-3} $cm^2/(V\ s)$.

Furthermore, electron-only devices[37] were fabricated to investigate the electron transport in the blends. The electron current is shown to be space charge limited in both devices and can therefore be analyzed with the Murgatroyd equation[38]

$$J = \frac{9}{8}\varepsilon_0\varepsilon_r\mu e^{0.89\beta\sqrt{(V-V_{bi})/d}}\frac{(V-V_{bi})^2}{d^3} \quad (6)$$

Figure 4 shows that the electron-only current density at a constant voltage is about 1 order of magnitude lower in the devices without DIO. According to eq 6, in the case of SCLC, the current density is directly proportional to the charge carrier mobility. This allows us to draw two important conclusions. First, as there is a large change in electron mobility upon addition of DIO but no difference in the mobility determined from the TDCF transient, the latter one can be assigned to holes. Second, the electron mobility in the devices without DIO is about 1 order of magnitude lower than the hole mobility, which will lead to severe extraction problems at low bias and limit the FF.

A fit to the data with eq 6 results in zero-field mobilities of about 5×10^{-4} and 5×10^{-6} $cm^2/(V\ s)$ for the device with and without DIO, respectively. However, mobility values obtained in this way have to be used with care, since the carrier densities in the space charge region at bias voltages larger than V_{OC} might well exceed the photogenerated charge carrier densities under solar illumination conditions. Also, different bottom electrodes are used for the electron-only devices and bipolar devices. Given that the nature of the bottom electrode might affect the blend morphology, electron mobilities in electron-only devices might differ from mobility values in the actual blend.

Therefore, in a third approach, electron mobilities were extracted from a fit to the entire TDCF transients at different delays and intensities with a transient drift-diffusion simulation (see Supporting Information for transient fits).[39] The electron mobility obtained therefrom with DIO is 3×10^{-4} $cm^2/(V\ s)$, which is in very good agreement with the single-carrier result. For the device without DIO, $\mu_e = 3 \times 10^{-5}$ $cm^2/(V\ s)$ was found which is 1 order of magnitude higher than the zero-field mobility from the single-carrier devices but very close to the mobility at short circuit ($\mu_{SC} = 1.3 \times 10^{-5}$ $cm^2/(V\ s)$). The reason for the discrepancy of the absolute values may lie in the different measurement conditions; however, the general trend of the mobility increasing with DIO is well reproduced.

Our findings are in part in variance with the results from the detailed mobility study by Foster et al.[16] While both studies agree that DIO has no effect on the hole mobility, the absolute values of electron and hole mobilities are significantly lower in ref 16. More importantly, Foster et al. found the electron mobility to decrease further with the use of DIO, despite a larger fill factor of the DIO-processed device. Here, we see no evidence for a lower electron mobility in blends with DIO. Also, as explained below and exemplified in Figure S8, Supporting Information (dashed line), we were not able to achieve good fits to our data using the mobility values of ref 16. Such low mobilities would significantly depress the fill factor. The reason for this discrepancy might, therefore, lie in a different morphology and different transport properties of the blend of PTB7 with $PC_{61}BM$ studied by Foster et al.[16]

As a conclusion to this section we note that the addition of DIO slightly reduces bimolecular recombination and at the same time increases the electron mobility. This moves the competition between recombination and extraction in favor of extraction and is responsible for the vast improvement of the device fill factor.

2.3. Numerical Simulations. In the next step a numerical drift-diffusion simulation[40] is used to examine whether the experimentally determined dynamic parameters are capable to explain the $J-V$ characteristics of the devices. In this simulation the density of states was set to the fixed value of 10^{27} m^{-3} and energetic disorder was neglected throughout all simulations. The metal work functions were aligned with the highest occupied molecular orbital (HOMO) and lowest unoccupied molecular orbital (LUMO) energies of the active layer, i.e., it was assumed that no significant injection and extraction barriers are present in the devices. Furthermore, as we have recently shown that the influence of surface recombination is negligible even in the presence of low bimolecular recombination rates in the order of $k = 1 \times 10^{-18}$ $m^3\ s^{-1}$,[17] infinite surface recombination was assumed in the simulations.

The dynamic quantities needed for a complete description of the $J-V$ characteristics are the charge carrier mobilities, charge generation, and recombination rates. The parameters that were used for the best fits at 1 sun illumination intensity are listed in Table 1. Note that all parameters used for the simulation were

DOI: 10.1021/jp512721e
J. Phys. Chem. C 2015, 119, 8310–8320

Table 1. Parameters Used for the Drift-Diffusion Simulation of the PTB7:PCBM Devices Prepared with and without DIO in Figure 5a and 5b

parameters	with DIO	without DIO
hole mobility	4.5×10^{-4} cm^2 V^{-1} s^{-1}	1.2×10^{-3} cm^2 V^{-1} s^{-1}
Poole–Frenkel factor	0	-0.002 cm$^{1/2}$V$^{-1/2}$
electron mobility	3×10^{-4} cm^2 V^{-1} s^{-1}	2.7×10^{-5} cm^2 V^{-1} s^{-1}
Poole–Frenkel factor	0	0
generation rate	1.1×10^{28} m^{-3} s^{-1}	6.5×10^{27} m^{-3} s^{-1} (at -0.7 V)
BMR coefficient	1.2×10^{-17} m^3 s^{-1}	4.5×10^{-17} m^3 s^{-1}
effective band gap	1.27 eV	1.36 eV

experimentally obtained from the same batch of PTB7 to avoid batch-to-batch variations that are sometimes observed in these blends. For the device with DIO a field-independent generation was assumed and the BMR coefficient was taken from the BACE experiments at high carrier density. The hole mobility was taken from the extrapolation of the TDCF transients (section 2.2), and the electron mobility was determined from a fit to the whole TDCF transients (Supporting Information). Figure 5a shows the experimental $J-V$ characteristics for the PTB7:PCBM devices prepared with DIO measured at different light intensities (symbols) together with the simulation results (solid lines). The excellent agreement of the simulation with the data for an intensity range covering 2 orders of magnitude

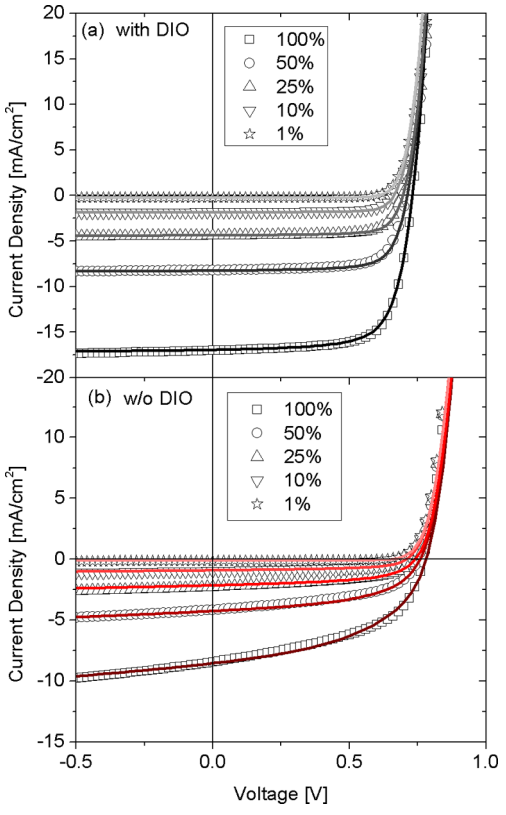

Figure 5. $J-V$ characteristics at different light intensities relative to 1 sun for the device prepared with (a) and without DIO (b). Symbols are the experimental data, and solid lines are drift-diffusion simulations (for more details see text). Simulation parameters are summarized in Tables 1 and 2.

indicates that a field-independent generation rate and a moderate bimolecular recombination rate with a carrier density-independent recombination coefficient in competition with efficient extraction of both electrons and holes sufficiently explains the $J-V$ characteristics. The generation rates used for the fits at different intensities are listed in Table 2.

Table 2. Generation Rates Used for the Fit of the $J-V$ Characteristics at Different Light Intensities in Figure 5[a]

intensity (1 sun)	with DIO	without DIO
100%	1.1×10^{28} m^{-3} s^{-1}	6.5×10^{27} m^{-3} s^{-1}
50%	5.3×10^{27} m^{-3} s^{-1}	3.2×10^{27} m^{-3} s^{-1}
25%	2.8×10^{27} m^{-3} s^{-1}	1.6×10^{27} m^{-3} s^{-1}
10%	1.2×10^{27} m^{-3} s^{-1}	6.7×10^{26} m^{-3} s^{-1}
1%	1.3×10^{26} m^{-3} s^{-1}	6.7×10^{25} m^{-3} s^{-1}

[a]For the devices without DIO the generation rate at -0.7 V is stated.

For the device without DIO a field-dependent generation was measured with TDCF (section 2.1). At this point the data from Figure 2a are considered for the numerical simulations as these measurements were taken on the same PTB7 batch as the $J-V$ curves in Figure 5. According to Figure 2a, the generation is fairly constant in the region from -2 to approximately -0.7 V and then drops by 20% from -0.7 to 0.7 V. This drop was approximated by a linear decrease. Using this parametrization, an effective generation rate was calculated for each bias voltage and taken as input parameter for the simulation. This approach differs from the generally used way to implement the dependence of the generation rate on the local electric field in form of the Braun–Onsager model.[41] Compared to this, our approach has two advantages. First, the parameters needed for the Braun–Onsager model are difficult to access by experiments and usually estimated from the drift-diffusion simulations themselves. Second, the field dependence measured with TDCF is an average over the entire active layer for each applied external bias, which is also relevant for the total current output of the device.

The hole mobility and the recombination coefficient were directly taken from the TDCF and BACE measurements, respectively. As direct measurements of the electron mobility yielded different values, we varied μ_e to give the best fit to the experimental curves, which happens to be very close to the value determined from the transient fit. The results for the experimental and simulated $J-V$ curves at five different illumination intensities are shown in Figure 5b, and the simulation parameters are listed in Tables 1 and 2. Again, very good agreement was achieved for all intensities for one set of parameters. Notably, a density-dependent mobility or recombination coefficient was not implemented to describe the $J-V$ characteristics, in accordance to the recombination data from TDCF. We therefore propose that the apparent density dependence of the nongeminate recombination coefficient in the devices without DIO seen in the BACE measurements is due to the disability of the method to account for an inhomogeneous charge carrier distribution within the active layer, which itself is caused by a rather coarse chain morphology and a low electron mobility.

In the simulation, the effective band gap, defined as the difference of the acceptor-LUMO and donor-HOMO energy, used for the simulations was chosen such that the simulated curve matches the experimental curve at V_{OC}. The resulting values were 1.27 and 1.36 eV for the devices with and without

DOI: 10.1021/jp512721e
J. Phys. Chem. C 2015, 119, 8310–8320

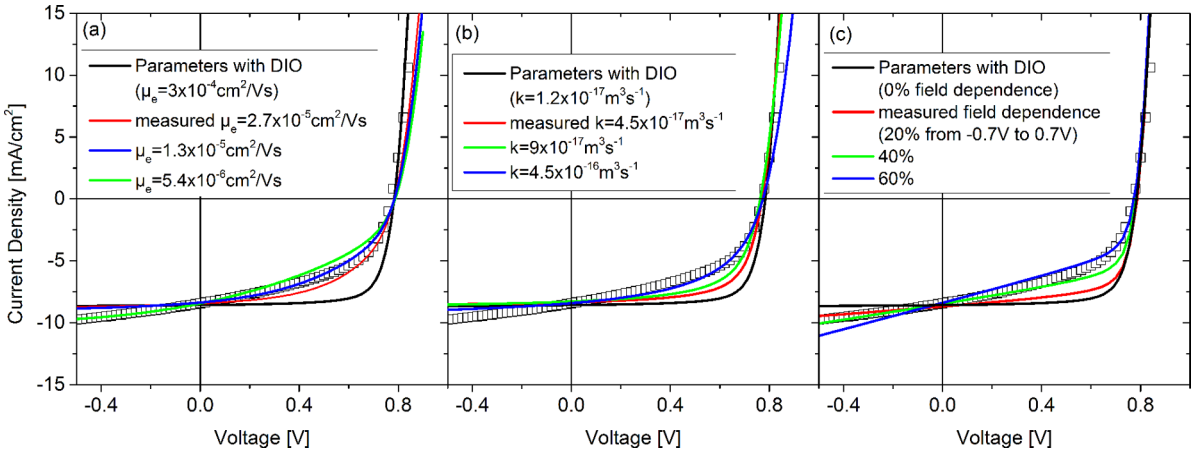

Figure 6. Experimental $J-V$ curves (symbols) for the blend without DIO, compared to parametric simulations (lines). In all curves, the black line displays the simulation with the parameters used for the device processed with DIO (see Table 1). Then only one parameter was altered, while all others were kept the same as in the DIO-processed case: In (a) only the electron mobility is stepwise reduced, in (b) only the BMR coefficient k is increased, and in (c) only the field dependence of generation is increased. In the simulations, the effective band gap and the generation rate (at −0.7 V) are adjusted to yield the same V_{OC} and J_{SC} for all curves. All other parameters are kept constant.

DIO, respectively. Effective band gaps determined with two different measurement techniques (see Supporting Information for details) are in very good agreement with the values used in the simulation and confirm the trend of a reduction of ca. 100 meV upon adding DIO, most likely caused by a change in domain morphology.

Importantly, the addition of DIO causes only minor to moderate changes of the individual dynamic parameters. Therefore, the variation of only one of these parameters cannot explain the dramatic improvement of the performance when DIO is added. This is demonstrated in Figure 6, where the experimental $J-V$ curves of the device without additive are compared to parametric simulations starting with the parameters used for the devices with DIO (black lines in Figure 6a−c). The generation rate (at −0.7 V) and the effective band gap were adjusted to achieve the same J_{SC} and V_{OC} for all simulated curves. As expected, this simulation leads to a much higher FF than was measured in devices without DIO. Then, only the electron mobility was stepwise reduced (Figure 6a), the BMR coefficient k was increased (Figure 6b), or the field dependence of generation was increased (Figure 6c). In each graph, the red lines show the simulation when using the value of the specific parameter as measured on the blend without additive, while the green and blue lines use values that further decrease the overall performance. Though in some cases parts of the $J-V$ curve are well resembled by the simulation, the applied parameters differ largely from the measured values. For example, the forth quadrant of the $J-V$ curve can be well fitted by only increasing the value of k to 4.5×10^{-16} m^3 s^{-1}, but this value is unrealistically large. Furthermore, these parameters fail to explain the $J-V$ characteristics over the full voltage range. The specific shape of the curve can, therefore, not be ascribed to the change of only the mobility, only the recombination, or only the field dependence of generation. Likewise, if the change of one of the parameters, e.g., the electron mobility, is neglected, the device FF and performance will be overestimated. It is only when the changes of all three parameters upon DIO addition are taken into account that the simulation matches the experimental $J-V$ characteristics under all illumination conditions and for a wide range of voltages.

3. CONCLUSION

We presented a conclusive and comprehensive study of the charge carrier dynamics in high efficiency PTB7:PCBM solar cells prepared with and without the solvent additive DIO. For the devices prepared with DIO all data can be consistently explained by the combination of a field-independent free charge carrier generation, a moderate bimolecular recombination with a carrier density-independent recombination coefficient, and efficient extraction of both electron and holes. The experimental results are consistent with a uniform morphology of well-interconnected donor and acceptor domains of the size of the exciton diffusion length.

For the devices prepared without DIO we find an overall reduced charge carrier generation efficiency. This is consistent with a structural model where large fullerene clusters are embedded into a polymer-rich surrounding. As already pointed out by Collins et al., this particular morphology will lead to inefficient exciton harvesting, due to a small active interface. Furthermore, the generation rate was found to be field dependent, in particular when exciting primarily the polymer. We propose that upon excitation of polymer excitons, CT excitations will primarily form at the interface to molecularly dispersed fullerenes and that these interfacial states are more prone to geminate recombination. In contrast, excitons generated in PCBM clusters appear to lead to more weakly bound CT excitons, located at the interface between pure fullerene aggregates and polymer chains. These findings demonstrate that the mechanism of free charge carrier generation depends largely on the specific local morphology of the blend and that it can be different if the light is absorbed primarily by the polymer or the fullerene component.

As a consequence of the very different morphologies, the device processed without the additive possesses distinctly different recombination dynamics, compared to devices with additive. BACE and TDCF consistently show a larger BMR coefficient k. Notably, our BACE experiments reveal an apparent dependence of k on charge carrier density. While this finding has been commonly explained by a density-dependent mobility, it might, alternatively, hint to an inhomogeneous spatial distribution of charge carriers in the device, as recently suggested by Deledalle et al.[31] In fact, our

DOI: 10.1021/jp512721e
J. Phys. Chem. C 2015, 119, 8310−8320

mobility measurements point to unbalanced charge transport in blends processed without the additive, due to a small electron mobility. Therefore, complementary measurements were performed with TDCF, which led to constant (density independent) recombination coefficients.

Most importantly, drift-diffusion simulations of the $J-V$ characteristics showed that the lower performance of the devices without DIO cannot be explained solely on the basis of a field-dependent generation or a higher coefficient for nongeminate recombination. Instead, the effect of the additive on the entire $J-V$ characteristics can only be reproduced when, in addition, taking into account a reduced electron mobility in the device processed without DIO, causing inefficient electron extraction and a poor fill factor. However, such a low electron mobility is in contrast to the simple morphology model of large, pure PCBM clusters in these blends, since electron transport is typically quite efficient in PCBM. This suggests that the true morphology might indeed be much more complex in blends without DIO. In fact, a more recent study by Hedley et al. showed that the large fullerene domains in the device without DIO (of 100−200 nm in diameter) consist of smaller 20−60 nm very pure fullerene spheres.[13] While the electron mobility within those small fullerene spheres might be quite high, the macroscopic transport across the entire fullerene domain could be limited by the transitions between the small spheres. Furthermore, it was also shown that PTB7:PCBM blends processed without additive can actually form a layered structure,[42] meaning that electrons will experience different morphologies when traveling across the entire active layer. Due to this very complex morphology structure in blends without DIO, which is still not fully understood, a conclusive interpretation of the influence of DIO on all photovoltaic parameters is yet not possible.

However, our work emphasizes the importance of considering all dynamic processes in the device. It especially highlights the importance of efficient charge extraction for reaching high currents and fill factors. Charge extraction is becoming an increasingly important topic, given the development of blends with internal quantum efficiencies of close to unity and concomitantly very high generation rates. The set of tools used in this work enables deep insight into the fundamental processes of high-efficiency organic solar cells and can be used to reveal the limiting factors of device performance of other material combinations.

4. EXPERIMENTAL DETAILS

4.1. Device Preparation. Solar cells were fabricated on structured indium tin oxide (ITO) glass substrates (Lumtec) coated with a 60 nm layer of PEDOT:PSS (Clevios AI 4083). PTB7 (purchased from 1-material) and $PC_{70}BM$ (purchased from Solenne) were separately solved in chlorobenzene (CB) and then mixed to a 1:1.5 (by weight) solution with a concentration of 25 g L^{-1} and subsequently spin coated at 1000 rpm, yielding an active layer thickness of 100 ± 5 nm. In the case of devices referred to as "with DIO" 3 vol % 1,8-diiodooctane (DIO) were used as cosolvent in the CB solution. Finally, 5 nm Ca and 80 nm Al were thermally evaporated through shadow masks, defining an active area of 1 mm^2. Such small area was used to avoid RC−time limitations in the transient measurements. All samples were encapsulated with epoxy resin and a glass lid prior to air exposure. Electron-only devices were prepared on Al-bottom electrodes and covered with Ca/Al-top electrodes, defining an active area of 5 mm^2. Different layer thicknesses were achieved by varying the solution concentration. All materials were used as received.

4.2. Measurements. The $J-V$ characteristics of the solar cells were measured with an Oriel class A simulator calibrated to 100 mW cm^{-2} and a Keithley 2400 sourcemeter under inert atmosphere. In the TDCF experiments pulsed excitation (5.5 ns pulse width, 500 Hz repetition rate) was realized with a diode-pumped, Q-switched neodymium-doped yttrium aluminum garnet (Nd:YAG) laser (NT242, EKSPLA). The photogenerated charge carriers were extracted by applying a high rectangular voltage pulse with a pulse generator (Agilent 81150A) in reverse direction. The current through the device was measured with an Agilent DSO9054H oscilloscope via a 50 Ω input resistor. For a detailed measurement scheme see ref 17. For BACE measurements an array of four focused white light LEDs (Lumileds Rebel, switch-off time < 200 ns) was used. While being illuminated the device was held at a fixed bias that corresponds exactly to the open-circuit voltage. When switching off the LEDs, the external bias was rapidly changed to reverse direction. The current due to electrode charging was subtracted by performing the same voltage jump in the dark, starting at 0 V. The $J-V$ characteristics of the electron-only devices were measured with a Keithley 2400 sourcemeter under inert atmosphere. Layer thicknesses were determined with a Dektak 3ST profilometer.

■ ASSOCIATED CONTENT

Supporting Information

$J-V$ curves with extended voltage range; total extracted charge measured with TDCF vs pulse fluence and extracted charge measured with BACE vs extraction bias; absorption spectra; measured and simulated TDCF transients; description of band gap determination. This material is available free of charge via the Internet at http://pubs.acs.org.

■ AUTHOR INFORMATION

Corresponding Author

*Phone: +49 331 977 1265. E-mail: neher@uni-potsdam.de.

Notes

The authors declare no competing financial interest.

■ ACKNOWLEDGMENTS

This work was supported by the German Science Foundation (DFG) within the priority program "Elementary Processes of Organic Photovoltaics" (SPP 1355), by the Helmholtz Energy Alliance for Hybrid Photovoltaics and by the BMBF (PVcomB).

■ REFERENCES

(1) He, Z.; Zhong, C.; Su, S.; Xu, M.; Wu, H.; Cao, Y. Enhanced Power-Conversion Efficiency in Polymer Solar Cells Using an Inverted Device Structure. *Nat. Photonics* **2012**, *6*, 591−595.

(2) Liang, Y.; Xu, Z.; Xia, J.; Tsai, S.-T.; Wu, Y.; Li, G.; Ray, C.; Yu, L. For the Bright Future—Bulk Heterojunction Polymer Solar Cells with Power Conversion Efficiency of 7.4%. *Adv. Mater.* **2010**, *22*, 135−138.

(3) Li, G.; Shrotriya, V.; Huang, J.; Yao, Y.; Moriarty, T.; Emery, K.; Yang, Y. High-Efficiency Solution Processable Polymer Photovoltaic Cells by Self-Organization of Polymer Blends. *Nat. Mater.* **2005**, *4*, 864−868.

(4) Savenije, T. J.; Kroeze, J. E.; Yang, X.; Loos, J. The Effect of Thermal Treatment on the Morphology and Charge Carrier Dynamics in a Polythiophene−Fullerene Bulk Heterojunction. *Adv. Funct. Mater.* **2005**, *15*, 1260−1266.

DOI: 10.1021/jp512721e
J. Phys. Chem. C 2015, 119, 8310−8320

(5) Nguyen, L. H.; Hoppe, H.; Erb, T.; Günes, S.; Gobsch, G.; Sariciftci, N. S. Effects of Annealing on the Nanomorphology and Performance of Poly(alkylthiophene):Fullerene Bulk-Heterojunction Solar Cells. *Adv. Funct. Mater.* **2007**, *17*, 1071−1078.
(6) Campoy-Quiles, M.; Ferenczi, T.; Agostinelli, T.; Etchegoin, P. G.; Kim, Y.; Anthopoulos, T. D.; Stavrinou, P. N.; Bradley, D. D. C.; Nelson, J. Morphology Evolution via Self-Organization and Lateral and Vertical Diffusion in Polymer:Fullerene Solar Cell Blends. *Nat. Mater.* **2008**, *7*, 158−164.
(7) Howard, I. A.; Mauer, R.; Meister, M.; Laquai, F. Effect of Morphology on Ultrafast Free Carrier Generation in Polythiophene:-Fullerene Organic Solar Cells. *J. Am. Chem. Soc.* **2010**, *132*, 14866−14876.
(8) Albrecht, S.; Janietz, S.; Schindler, W.; Frisch, J.; Kurpiers, J.; Kniepert, J.; Inal, S.; Pingel, P.; Fostiropoulos, K.; Koch, N.; et al. Fluorinated Copolymer PCPDTBT with Enhanced Open-Circuit Voltage and Reduced Recombination for Highly Efficient Polymer Solar Cells. *J. Am. Chem. Soc.* **2012**, *134*, 14932−14944.
(9) Chen, W.; Xu, T.; He, F.; Wang, W.; Wang, C.; Strzalka, J.; Liu, Y.; Wen, J.; Miller, D. J.; Chen, J.; et al. Hierarchical Nanomorphologies Promote Exciton Dissociation in Polymer/Fullerene Bulk Heterojunction Solar Cells. *Nano Lett.* **2011**, *11*, 3707−3713.
(10) Hammond, M. R.; Kline, R. J.; Herzing, A. A.; Richter, L. J.; Germack, D. S.; Ro, H.-W.; Soles, C. L.; Fischer, D. A.; Xu, T.; Yu, L.; et al. Molecular Order in High-Efficiency Polymer/Fullerene Bulk Heterojunction Solar Cells. *ACS Nano* **2011**, *5*, 8248−8257.
(11) Collins, B. A.; Li, Z.; Tumbleston, J. R.; Gann, E.; McNeill, C. R.; Ade, H. Absolute Measurement of Domain Composition and Nanoscale Size Distribution Explains Performance in PTB7:PC71BM Solar Cells. *Adv. Energy Mater.* **2013**, *3*, 65−74.
(12) Liu, F.; Zhao, W.; Tumbleston, J. R.; Wang, C.; Gu, Y.; Wang, D.; Briseno, A. L.; Ade, H.; Russell, T. P. Understanding the Morphology of PTB7:PCBM Blends in Organic Photovoltaics. *Adv. Energy Mater.* **2014**, *4*, 1301377.
(13) Hedley, G. J.; Ward, A. J.; Alekseev, A.; Howells, C. T.; Martins, E. R.; Serrano, L. A.; Cooke, G.; Ruseckas, A.; Samuel, I. D. W. Determining the Optimum Morphology in High-Performance Polymer-Fullerene Organic Photovoltaic Cells. *Nat. Commun.* **2013**, *4*, 2867.
(14) Li, Z.; Lakhwani, G.; Greenham, N. C.; McNeill, C. R. Voltage-Dependent Photocurrent Transients of PTB7:PC70BM Solar Cells: Experiment and Numerical Simulation. *J. Appl. Phys.* **2013**, *114*, 034502−034508.
(15) Foertig, A.; Kniepert, J.; Gluecker, M.; Brenner, T.; Dyakonov, V.; Neher, D.; Deibel, C. Nongeminate and Geminate Recombination in PTB7:PCBM Solar Cells. *Adv. Funct. Mater.* **2014**, *24*, 1306−1311.
(16) Foster, S.; Deledalle, F.; Mitani, A.; Kimura, T.; Kim, K.-B.; Okachi, T.; Kirchartz, T.; Oguma, J.; Miyake, K.; Durrant, J. R.; et al. Electron Collection as a Limit to Polymer:PCBM Solar Cell Efficiency: Effect of Blend Microstructure on Carrier Mobility and Device Performance in PTB7:PCBM. *Adv. Energy Mater.* **2014**, *4*, 1400311−1400323.
(17) Kniepert, J.; Lange, I.; van der Kaap, N. J.; Koster, L. J. A.; Neher, D. A Conclusive View on Charge Generation, Recombination, and Extraction in As-Prepared and Annealed P3HT:PCBM Blends: Combined Experimental and Simulation Work. *Adv. Energy Mater.* **2014**, *4*, 1301401.
(18) Credgington, D.; Jamieson, F. C.; Walker, B.; Nguyen, T.-Q.; Durrant, J. R. Quantification of Geminate and Non-Geminate Recombination Losses within a Solution-Processed Small-Molecule Bulk Heterojunction Solar Cell. *Adv. Mater.* **2012**, *24*, 2135−2141.
(19) Kniepert, J.; Schubert, M.; Blakesley, J. C.; Neher, D. Photogeneration and Recombination in P3HT/PCBM Solar Cells Probed by Time-Delayed Collection Field Experiments. *J. Phys. Chem. Lett.* **2011**, *2*, 700−705.
(20) Albrecht, S.; Schindler, W.; Kurpiers, J.; Kniepert, J.; Blakesley, J. C.; Dumsch, I.; Allard, S.; Fostiropoulos, K.; Scherf, U.; Neher, D. On the Field Dependence of Free Charge Carrier Generation and Recombination in Blends of PCPDTBT/PC70BM: Influence of Solvent Additives. *J. Phys. Chem. Lett.* **2012**, *3*, 640−645.
(21) Gluecker, M.; Foertig, A.; Dyakonov, V.; Deibel, C. Impact of Nongeminate Recombination on the Performance of Pristine and Annealed P3HT:PCBM Solar Cells. *Phys. Status Solidi RRL* **2012**, *6*, 337−339.
(22) Brenner, T. J. K.; Li, Z.; McNeill, C. R. Phase-Dependent Photocurrent Generation in Polymer/Fullerene Bulk Heterojunction Solar Cells. *J. Phys. Chem. C* **2011**, *115*, 22075−22083.
(23) Jamieson, F. C.; Domingo, E. B.; McCarthy-Ward, T.; Heeney, M.; Stingelin, N.; Durrant, J. R. Fullerene Crystallisation as a Key Driver of Charge Separation in Polymer/Fullerene Bulk Heterojunction Solar Cells. *Chem. Sci.* **2012**, *3*, 485−492.
(24) Gélinas, S.; Rao, A.; Kumar, A.; Smith, S. L.; Chin, A. W.; Clark, J.; van der Poll, T. S.; Bazan, G. C.; Friend, R. H. Ultrafast Long-Range Charge Separation in Organic Semiconductor Photovoltaic Diodes. *Science* **2013**, *343*, 512.
(25) Savoie, B. M.; Rao, A.; Bakulin, A. A.; Gelinas, S.; Movaghar, B.; Friend, R. H.; Marks, T. J.; Ratner, M. A. Unequal Partnership: Asymmetric Roles of Polymeric Donor and Fullerene Acceptor in Generating Free Charge. *J. Am. Chem. Soc.* **2014**, *136*, 2876−2884.
(26) Zusan, A.; Vandewal, K.; Allendorf, B.; Hansen, N. H.; Pflaum, J.; Salleo, A.; Dyakonov, V.; Deibel, C. The Crucial Influence of Fullerene Phases on Photogeneration in Organic Bulk Heterojunction Solar Cells. *Adv. Energy Mater.* **2014**, 1400922.
(27) Shuttle, C. G.; Hamilton, R.; Nelson, J.; O'Regan, B. C.; Durrant, J. R. Measurement of Charge-Density Dependence of Carrier Mobility in an Organic Semiconductor Blend. *Adv. Funct. Mater.* **2010**, *20*, 698−702.
(28) Rauh, D.; Deibel, C.; Dyakonov, V. Charge Density Dependent Nongeminate Recombination in Organic Bulk Heterojunction Solar Cells. *Adv. Funct. Mater.* **2012**, *22*, 3371−3377.
(29) Lange, I.; Kniepert, J.; Pingel, P.; Dumsch, I.; Allard, S.; Janietz, S.; Scherf, U.; Neher, D. Correlation between the Open Circuit Voltage and the Energetics of Organic Bulk Heterojunction Solar Cells. *J. Phys. Chem. Lett.* **2013**, *4*, 3865−3871.
(30) Shuttle, C. G.; O'Regan, B.; Ballantyne, A. M.; Nelson, J.; Bradley, D. D. C.; Durrant, J. R. Bimolecular Recombination Losses in Polythiophene:Fullerene Solar Cells. *Phys. Rev. B* **2008**, *78*, 113201.
(31) Deledalle, F.; Shakya Tuladhar, P.; Nelson, J.; Durrant, J. R.; Kirchartz, T. Understanding the Apparent Charge Density Dependence of Mobility and Lifetime in Organic Bulk Heterojunction Solar Cells. *J. Phys. Chem. C* **2014**, *118*, 8837−8842.
(32) Clarke, T. M.; Jamieson, F. C.; Durrant, J. R. Transient Absorption Studies of Bimolecular Recombination Dynamics in Polythiophene/Fullerene Blend Films. *J. Phys. Chem. C* **2009**, *113*, 20934−20941.
(33) Kirchartz, T.; Nelson, J. Meaning of Reaction Orders in Polymer:Fullerene Solar Cells. *Phys. Rev. B* **2012**, *86*, 165201.
(34) Deibel, C.; Wagenpfahl, A.; Dyakonov, V. Origin of Reduced Polaron Recombination in Organic Semiconductor Devices. *Phys. Rev. B* **2009**, *80*, 075203.
(35) Blakesley, J. C.; Castro, F. A.; Kylberg, W.; Dibb, G. F. A.; Arantes, C.; Valaski, R.; Cremona, M.; Kim, J. S.; Kim, J.-S. Towards Reliable Charge-Mobility Benchmark Measurements for Organic Semiconductors. *Org. Electron.* **2014**, *15*, 1263−1272.
(36) Cowan, S. R.; Street, R. A.; Cho, S.; Heeger, A. J. Transient Photoconductivity in Polymer Bulk Heterojunction Solar Cells: Competition between Sweep-out and Recombination. *Phys. Rev. B* **2011**, *83*, 035205.
(37) Blom, P. W. M.; de Jong, M. J. M.; van Munster, M. G. Electric-Field and Temperature Dependence of the Hole Mobility in Poly(p-phenylene vinylene). *Phys. Rev. B* **1997**, *55*, R656−R659.
(38) Murgatroyd, P. N. Theory of Space-Charge-Limited Current Enhanced by Frenkel Effect. *J. Phys. D: Appl. Phys.* **1970**, *3*, 151.
(39) Bange, S. Transient Optical and Electrical Effects in Polymeric Semiconductors. Ph.D. Thesis, University of Potsdam, Germany, 2009.

DOI: 10.1021/jp512721e
J. Phys. Chem. C 2015, 119, 8310−8320

(40) Koster, L. J. A.; Smits, E. C. P.; Mihailetchi, V. D.; Blom, P. W. M. Device Model for the Operation of Polymer/Fullerene Bulk Heterojunction Solar Cells. *Phys. Rev. B* **2005**, *72*, 085205.
(41) Braun, C. L. Electric Field Assisted Dissociation of Charge Transfer States as a Mechanism of Photocarrier Production. *J. Chem. Phys.* **1984**, *80*, 4157−4161.
(42) Wang, D.; Liu, F.; Yagihashi, N.; Nakaya, M.; Ferdous, S.; Liang, X.; Muramatsu, A.; Nakajima, K.; Russel, T. P. New Insights into Morphology of High Performance BHJ Photovoltaics Revealed by High Resolution AFM. *Nano Lett.* **2014**, *14*, 5727−5732.

DOI: 10.1021/jp512721e
J. Phys. Chem. C 2015, 119, 8310−8320